THE ASTROPHYSICAL JOURNAL, 561:346–363, 2001 November 1

NEUTRON CAPTURE ELEMENTS IN *s*-PROCESS–RICH, VERY METAL-POOR STARS

WAKO AOKI,[1] SEAN G. RYAN,[2] JOHN E. NORRIS,[3] TIMOTHY C. BEERS,[4] HIROYASU ANDO,[1,5] NOBUYUKI IWAMOTO,[1,6] TOSHITAKA KAJINO,[1,5] GRANT J. MATHEWS,[7] AND MASAYUKI Y. FUJIMOTO[8]

Received 2001 April 6; accepted 2001 July 9

ABSTRACT

We report abundance estimates for neutron capture elements, including lead (Pb), and nucleosynthesis models for their origin, in two carbon-rich, very metal-poor stars, LP 625-44 and LP 706-7. These stars are subgiants whose surface abundances are likely to have been strongly affected by mass transfer from companion asymptotic giant branch (AGB) stars that have since evolved to white dwarfs. The detections of Pb, which forms the final abundance peak of the *s*-process, enable a comparison of the abundance patterns from Sr ($Z = 38$) to Pb ($Z = 82$) with predictions of AGB models. The derived chemical compositions provide strong constraints on the AGB stellar models, as well as on *s*-process nucleosynthesis at low metallicity. The present paper reports details of the abundance analysis for 16 neutron capture elements in LP 625-44, including the effects of hyperfine splitting and isotope shifts of spectral lines for some elements. A Pb abundance is also derived for LP 706-7 by a reanalysis of a previously observed spectrum. We investigate the characteristics of the nucleosynthesis pathway that produces the abundance ratios of these objects using a parametric model of the *s*-process without adopting any specific stellar model. The neutron exposure τ is estimated to be about 0.7 mbarn^{-1}, significantly larger than that which best fits solar system material, but consistent with the values predicted by models of moderately metal-poor AGB stars. This value is strictly limited by the Pb abundance, in addition to those of Sr and Ba. We also find that the observed abundance pattern can be explained by a few recurrent neutron exposures and that the overlap of the material that is processed in two subsequent exposures is small (the overlap factor $r \sim 0.1$).

Subject headings: nuclear reactions, nucleosynthesis, abundances — stars: abundances — stars: AGB and post-AGB — stars: carbon — stars: Population II

On-line material: color figures, machine-readable tables

1. INTRODUCTION

Many efforts have been made to explain the solar system abundances of elements associated with the slow neutron capture process (*s*-process). One common approach is the so-called classical model, which assumes an exponential distribution of neutron exposures (Käppeler, Beer, & Wisshak 1989). Use of this approach led to the conclusion that three distinct distributions of neutron exposures are required to represent solar system *s*-process abundances. One is referred to as the main component, thought to be responsible for most of the isotopes of *s*-process origin with $90 < A < 204$ (A indicates the mass number). Since the elements with $A < 90$ cannot be explained by the main component alone, another distribution, with lower neutron exposure, was introduced (the so-called weak component). The sites of the main and weak *s*-processes are believed to be thermally pulsing asymptotic giant branch (AGB) stars and helium core burning massive stars, respectively. The solar system abundances of the heaviest nuclei, with $204 \leq A \leq 209$, most of which are isotopes of Pb, cannot be reproduced by these two components, so the third so-called strong component with very high neutron exposure was introduced.

While this simple approach has been somewhat successful in explaining the solar system *s*-process abundances, detailed models of nucleosynthesis in thermally pulsing AGB stars have also been studied in attempts to confront the data with specific predictions from the likely production site. Recent modeling of AGB stars by Straniero et al. (1995) showed that neutron capture mainly occurs, not in the convective He shell during a thermal pulse, but in the radiative state between two given pulses. In this model the density distribution of the ^{13}C-rich layer (referred to as the ^{13}C pocket), which provides neutrons for the *s*-process, is taken as a free parameter. Since, in this case, the distribution of neutron exposures cannot be approximated by an exponential, the yields of neutron capture elements have been systematically calculated based on the stellar models by Gallino et al. (1998) and Arlandini et al. (1999), who succeeded in reproducing at least the main component of the solar system *s*-process elements.

In the Torino AGB models mentioned above, the ^{13}C pocket is generated artificially and described parametrically, assuming that some (poorly characterized) mixing of the overlying H-rich layers down into the He-rich intershell region occurs. A different approach to this problem is taken

[1] National Astronomical Observatory, Mitaka, Tokyo 181-8588, Japan; aoki.wako@nao.ac.jp, ando@optik.mtk.nao.ac.jp, iwamoto@th.nao.ac.jp, kajino@nao.ac.jp.
[2] Department of Physics and Astronomy, The Open University, Walton Hall, Milton Keynes, MK7 6AA, UK; s.g.ryan@open.ac.uk.
[3] Research School of Astronomy and Astrophysics, The Australian National University, Private Bag, Weston Creek Post Office, Canberra, ACT 2611, Australia; jen@mso.anu.edu.au.
[4] Department of Physics and Astronomy, Michigan State University, East Lansing, MI 48824-1116; beers@pa.msu.edu.
[5] Department of Astronomy, Graduate School of Science, University of Tokyo, Bunkyo-ku, Tokyo 113-0033, Japan.
[6] Center for Nuclear Study, University of Tokyo, Wako, Saitama 351-0198, Japan.
[7] Department of Physics and Center for Astrophysics, University of Notre Dame, Notre Dame, IN 46556; gmathews@nd.edu.
[8] Department of Physics, Hokkaido University, Sapporo, Hokkaido 060-0810, Japan; fujimoto@astro1.sci.hokudai.ac.jp.

by the Geneva group, who model the mixing process via a diffusion mechanism (e.g., Goriely & Mowlavi 2000). Whichever approach is taken—parameterization of the ^{13}C pocket by the Torino group or parameterization of mixing by the Geneva group—fundamental uncertainties currently exist in the models. It is in the spirit of improving our understanding of these stars, rather than confronting or endorsing any particular approach to modeling, that we present the following analysis.

The calculation of *s*-process yields was extended to lower metallicity by Gallino et al. (1998), and a systematic investigation was performed by Busso, Gallino, & Wasserburg (1999). Since the difference in metallicity of the model affects the ratio of neutrons to seed nuclei, the distribution of *s*-process elements produced in AGB stars should be sensitive to the metallicity as well. While the abundance of seed nuclei (most of which are iron) is proportional to the metallicity, the production of ^{13}C (the main neutron source) is expected to be metallicity independent. Consequently, higher abundances of heavier elements are expected in the yields of AGB stars with lower metallicity. The calculations of Gallino et al. (1998) and Busso et al. (1999) indeed predict higher abundance ratios of heavy to light *s*-process elements, and very high Pb and Bi abundances, in the nucleosynthesis products of metal-poor AGB stars. Moreover, they suggested that the origin of Pb, and hence the site of the strong component of the *s*-process, should be attributed to these metal-poor AGB stars.

The nucleosynthesis of heavy elements in metal-poor AGB stars can be investigated by abundance studies of carbon-rich and *s*-process–rich objects, often referred to as CH stars, whose surface chemical composition is considered to result from mass transfer from a now-extinct AGB companion. In one such star, LP 625-44, a Pb I line was detected by Aoki et al. (2000, hereafter Paper I) for the first time (in a CH star), and it became possible to compare abundance ratios for elements from Sr to Pb with model predictions. LP 625-44 is an ideal object for this study. One reason is that it is very metal-poor ([Fe/H] $= -2.7$) and shows very high *s*-process overabundances (e.g., [Ba/Fe] $= 2.7$), so the abundances of heavy elements almost purely represent the yields of the AGB donor (see § 4.1). Another reason is that the variation of radial velocity, with a period longer than 12 yr (as found by our monitoring), strongly supports the mass transfer scenario. The Pb abundance derived is, however, much lower than the prediction by the standard model of Busso et al. (1999). This result provides a strong constraint on the nature of the ^{13}C pocket, which is a parameter in their model (Ryan et al. 2001), and may even prompt reconsideration of models of *s*-process nucleosynthesis in very metal-poor AGB stars. Clearly, the study of elemental abundances in these objects is important for investigation of the origin of Pb in the solar system.

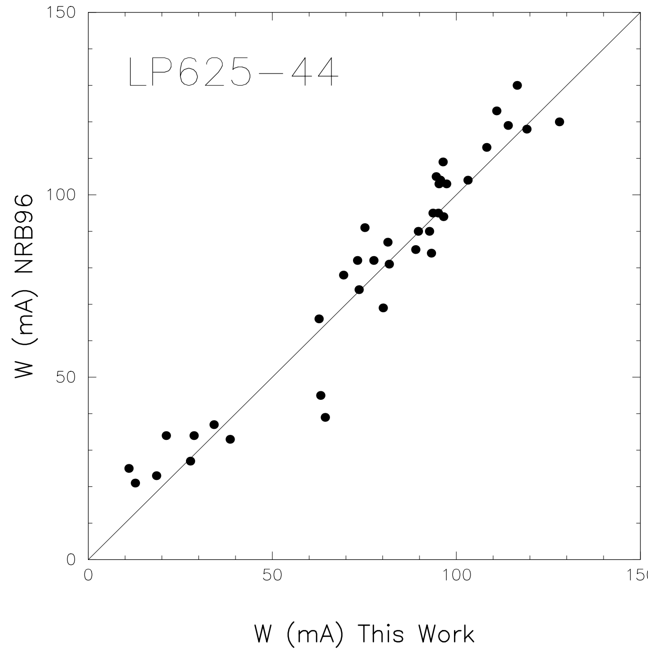

FIG. 1.—Comparison of the equivalent widths measured by the present analysis with those of Norris et al. (1997a).

In this paper we report details of the abundance analysis of LP 625-44 that was summarized in Paper I and reanalyze an extended line list. For the analysis of many lines of neutron capture elements, the effects of hyperfine splitting and isotope shifts are taken into consideration. The line data and these additional effects are described in § 3 and in Appendix A. We also analyze another *s*-process–rich, very metal-poor star, LP 706-7, previously studied by Norris, Ryan, & Beers (1997a), and determine its Pb abundance for the first time (§ 3). In § 4 we discuss the characteristics of the nucleosynthesis that produces the abundance ratios of these objects by a parametric model of the *s*-process, without reference to any specific stellar model.

2. OBSERVATION AND MEASUREMENTS

LP 625-44 and LP 706-7 were observed with the University College London coudé echelle spectrograph (UCLES) and Tektronix 1024 × 1024 CCD at the Anglo-Australian Telescope. Our UV–blue spectra cover the wavelength region from 3700 to 4700 Å. A red spectrum (5000–7800 Å) was also obtained for LP 625-44. The observational and data reduction procedures have already been reported in Paper I for LP 625-44 and in Norris et al. (1997a) for LP 706-7. Details of the observations are summarized in Table 1. We note that the numbers of photons

TABLE 1

OBSERVATIONS

Object	R.A.(1950)	Decl.(1950)	V	$B-V$	Observation Date
LP 625-44......	16 40 38	−01 49 42	11.85	0.69	1996 Oct 21
LP 706-7	00 41 33	−14 11 36	12.11	0.46	1994–1996[a]

NOTE.—Units of right ascension are hours, minutes, and seconds, and units of declination are degrees, arcminutes, and arcseconds.

[a] 1994 May 29 and 31, 1994 October 24 and 25, and 1996 September 24.

TABLE 2

EQUIVALENT WIDTHS MEASURED FOR LINES OF NEUTRON CAPTURE ELEMENTS IN LP 625-44

λ (Å)	χ (eV)	log *gf*	*W* (mÅ)	log ϵ	δ(log ϵ)	Reference
			Sr II			
4077.71	0.00	0.150	151.99	1.33	...	1
4161.80	2.94	−0.500	7.55	1.53	...	1
4215.52	0.00	−0.170	123.70	1.27	...	1
			Y II			
3818.34	0.13	−0.980	35.48	0.67	...	1
3950.36	0.10	−0.490	45.73	0.37	...	1
			Zr II			
4208.98	0.71	−0.460	39.97	1.27	...	2
4258.05	0.56	−1.130	16.86	1.20	...	2
4443.00	1.49	−0.330	13.73	1.25	...	2
4496.97	0.71	−0.810	27.67	1.30	...	2
			Ba II			
5853.69	0.60	−1.010	110.05	2.28	<0.01	1
6141.73	0.70	−0.070	176.98	2.21	≤0.01	1
6496.91	0.60	−0.380	164.53	2.28	≤0.02	1
			La II			
3790.83[a]	0.13	0.143	75.33	0.94	0.06:	3
3949.10[a]	0.40	0.615	132.32	0.44	1.52:	3
3988.52[a]	0.40	0.080	119.38	0.80	1.50:	1
3995.75[a]	0.17	−0.020	87.57	0.70	0.81	1
4086.71[a]	0.00	−0.160	72.14	0.68	0.33:	1
4123.23[a]	0.32	0.120	78.06	1.16	0.01:	1
4238.38[a]	0.40	−0.085	106.21	0.88	1.52:	3
4322.51	0.17	−1.050	54.94	1.15	0.33	3
4333.76[a]	0.17	−0.160	125.73	1.21	1.12:	1
4429.90[a]	0.23	−0.370	118.90	1.80	0.68:	3
4558.46	0.32	−1.020	35.52	1.07	0.03	3
4574.88	0.17	−1.120	35.13	0.87	0.16	3
4613.39	0.71	−0.467	38.48	1.01	0.01:	3
4662.51	0.00	−1.280	40.59	1.02	0.10:	3
			Ce II			
3855.29	0.52	0.000	15.95	0.66	≤0.01:	4
3904.34	0.55	−0.390	17.60	1.13	≤0.01:	4
3909.31	0.45	−0.520	10.71	0.87	≤0.01:	4
3940.64	0.49	−0.920	8.86	1.23	≤0.01:	4
3980.88	0.71	0.030	15.89	0.80	≤0.01:	4
3984.68	0.96	0.410	13.41	0.60	≤0.01:	4
3992.91	0.73	−0.130	15.66	0.98	≤0.01:	4
4011.56	0.71	−0.740	11.09	1.38	≤0.01:	4
4015.88	1.04	0.000	15.55	1.17	≤0.01:	4
4062.22	1.37	0.350	19.32	1.27	≤0.01:	4
4065.16	0.90	−0.640	17.28	1.71	≤0.01:	4
4070.84	1.53	−0.090	12.26	1.64	≤0.01:	4
4076.24	0.81	−0.340	12.58	1.14	≤0.01:	4
4117.29	0.74	−0.450	8.53	0.98	≤0.01:	4
4119.02	0.55	−0.530	19.01	1.28	≤0.01:	4
4148.90	1.09	0.040	17.94	1.24	≤0.01:	4
4185.33	0.42	−0.560	18.32	1.14	≤0.01:	4
4190.63	0.90	−0.390	20.68	1.55	≤0.01:	4
4193.87	0.55	−0.400	10.77	0.84	≤0.01:	4
4257.12	0.46	−1.020	9.45	1.29	≤0.01:	4
4427.92	0.54	−0.380	22.01	1.17	≤0.01:	4
4444.70	1.06	0.100	20.55	1.20	≤0.01:	4
4485.52	0.98	−0.720	19.48	1.89	≤0.01:	4
4515.86	1.06	−0.520	9.78	1.41	≤0.01:	4

TABLE 2—*Continued*

λ (Å)	χ (eV)	log *gf*	*W* (mÅ)	log ϵ	δ(log ϵ)	Reference
4544.96	0.42	−0.890	19.49	1.46	≤0.01:	4
4551.30	0.74	−0.490	21.05	1.45	≤0.01:	4
			Pr II			
3918.86[a]	0.37	0.260	26.36	0.21	0.26	4
3925.47	0.00	−0.330	15.37	0.16	0.34	5
3964.26[a]	0.22	−0.330	46.29	0.95	0.30	4
3964.81[a]	0.05	0.090	52.95	0.38	0.45	5
3965.25[a]	0.20	−0.130	54.78	0.78	0.48	5
3997.04[a]	0.37	−0.100	22.11	0.62	0.02	5
4008.69[a]	0.63	0.590	40.96	0.37	0.26	4
4056.54[a]	0.63	0.640	30.87	0.16	0.28	4
4143.14[a]	0.37	0.380	64.30	0.53	0.64	5
4148.44	0.22	−0.720	5.05	0.25	0.07	4
4171.82	0.37	−0.340	21.52	0.68	0.11	4
4405.83[a]	0.55	−0.350	59.84	0.94	0.51	5
4535.92	0.00	−0.980	15.11	0.73	0.06	4
4651.50	0.20	−1.030	14.25	0.95	0.06	4
			Nd II			
3780.40[a]	0.47	−0.270	29.6	1.04	0.00	6
3941.51[a]	0.06	0.150	54.0	0.77	0.03	6
3979.49[a]	0.20	−0.110	40.9	0.83	0.01	6
4061.09[a]	0.47	0.300	63.1	1.15	0.15	6
4133.36[a]	0.32	−0.340	34.9	1.01	0.02	6
4446.39[a]	0.20	−0.630	39.0	1.23	0.02	7
4451.57[a]	0.38	0.020	54.6	1.04	0.12	6
4462.99[a]	0.56	−0.070	58.3	1.39	0.15	6
			Sm II			
3922.40	0.38	0.090	15.49	−0.12	0.00	4
3941.87	0.00	−0.590	11.62	0.01	...	4
3979.20	0.54	−0.190	18.41	0.43	0.00	4
4220.66	0.54	−0.400	7.08	0.12	0.00	4
4244.70	0.28	−0.730	12.85	0.46	0.00	8
4318.94[a]	0.28	−0.270	22.67	0.29	0.02	8
4424.34[a]	0.49	0.065	38.20	0.48	0.08	4
4433.88[a]	0.43	−0.260	41.08	0.90	0.00	4
4434.32[a]	0.38	−0.260	31.00	0.56	0.05	4
4458.52	0.10	−0.780	16.19	0.41	0.02	4
4499.48	0.25	−1.000	9.01	0.49	0.00	8
4536.51	0.10	−1.390	8.20	0.63	...	4
4537.95[a]	0.49	−0.230	21.02	0.38	0.04	8
4543.95[a]	0.33	−0.680	18.48	0.63	0.00	4
4552.66	0.25	−1.060	14.38	0.78	0.00	4
4566.21	0.33	−0.920	18.09	0.86	0.00	4
4577.69	0.25	−0.770	20.61	0.69	0.00	8
4584.83	0.43	−0.750	22.37	0.92	0.00	4
4593.54	0.38	−0.980	16.83	0.92	...	4
4595.29	0.49	−0.710	11.17	0.55	...	4
4642.24[a]	0.38	−0.520	32.31	0.84	0.03	8
4674.60	0.18	−0.560	15.04	0.22	0.01	4
4687.18	0.04	−1.170	19.47	0.78	0.05	4
			Eu II			
3907.10	0.21	0.196	52.0[b]	−0.15	≤0.15	1
4522.57	0.21	−0.678	12.5[b]	−0.30	≤0.1	1
			Gd II			
3844.58	0.14	−0.510	19.33	0.53	...	4
3957.67	0.60	−0.220	25.25	0.87	...	4
4070.29	0.56	−0.510	9.05	0.53	...	4

TABLE 2—*Continued*

λ (Å)	χ (eV)	log *gf*	*W* (mÅ)	log ϵ	δ(log ϵ)	Reference
4073.20	0.43	−0.700	23.41	1.11	...	4
4085.56	0.73	0.070	17.13	0.47	...	9
4215.02	0.43	−0.580	14.35	0.69	...	4
			Dy II			
3757.37	0.10	−0.140	27.6[b]	0.1	...	10
3944.68	0.00	0.075	45.8[b]	0.2	...	10
3996.69	0.59	−0.180	16.3[b]	0.3	...	10
4077.96	0.10	−0.025	22.4[b]	−0.2	...	10
			Er II			
3786.84	0.00	−0.640	29.4[b]	0.4	...	1
3938.63	0.00	−0.520	31.1[b]	0.3	...	1
			Tm II			
3700.26	0.03	−0.290	14.6[b]	−0.6	...	1
			Hf II			
3918.09	0.45	−1.260	11.0[b]	0.6	...	1
4093.16	0.45	−1.390	20.0[b]	0.9	...	1
			Pb I			
4057.815......	1.32	−0.20	24.0[b]	1.9	0.1	11

NOTE.—Table 2 is also available in machine-readable form in the electronic edition of the *Astrophysical Journal.*

[a] Lines that were added in the present analysis to the lines studied in Paper I.

[b] Synthesized value calculated for the abundance derived by spectrum synthesis.

REFERENCES.—(1) Sneden et al. 1996. (2) Biémont et al. 1981. (3) Bord et al. 1996. (4) Corliss & Bozman 1962. (5) Goly et al. 1991. (6) Maier & Whaling 1977. (7) Ward et al. 1985. (8) Biémont et al. 1989. (9) Bergström et al. 1988. (10) Kusz 1992. (11) Youssef & Khalil 1989.

obtained around Pb I λ4057 are 8800 per 0.04 Å pixel (signal-to-noise ratio S/N ∼ 150 per resolution element) and 3000 per 0.04 Å pixel (S/N ∼ 80) for LP 625-44 and LP 706-7, respectively.

For LP 625-44, equivalent widths were measured for most elements by fitting Gaussian profiles to the absorption lines. In Figure 1 the equivalent widths of Fe I, measured in the present work, are compared with those in Norris, Ryan, & Beers (1996), which were based on earlier spectra. There is no systematic difference between the two. We note that the S/N ratio in this work is about twice that in Norris et al. (1996). The equivalent widths measured for the lines of neutron capture elements in LP 625-44 are listed in Table 2. For the elements Eu, Dy, Er, Tm, Hf, and Pb, the abundances were derived by spectrum synthesis. The equivalent widths given for these elements (marked by a footnote) in the table are the synthesized values that are calculated for the abundance derived in our analysis.

3. ABUNDANCE ANALYSIS AND RESULTS

3.1. *Stellar Atmosphere Parameters*

We carried out a standard abundance analysis based on the equivalent widths and spectrum synthesis using model atmospheres in the ATLAS grid of Kurucz (1993). The stellar parameters have already been reported in Paper I for LP 625-44. For the analysis of Pb I lines in LP 706-7, the parameters determined by Norris et al. (1997a) were adopted. For convenience, we summarize the stellar parameters (effective temperature $T_{\rm eff}$, surface gravity g, microturbulent velocity v, and iron abundance) in Table 3.

The surface gravity of LP 706-7 (Norris et al. 1997a) was based on the requirement that Fe I and Fe II lines give identical abundances. More recently, a trigonometric parallax for this star has been published from the *Hipparcos* mission (ESA 1997), $\pi = 15.15 \pm 3.24$ mas. Somewhat surprisingly, this surface gravity indicates an absolute magnitude $M_V = 8.0 \pm 0.4$, which is subluminous compared to both main-sequence and subgiant Population II stars with $T_{\rm eff} = 6000$ K. A subgiant of $M_V = 3.0$ or 4.0 would have a parallax of only 1.5 or 2.4 mas. Either the *Hipparcos* measurement of this star is significantly in error, or the star is far more bizarre than its CH star status suggests. If the temperature estimate (based on photometric colors) and the *Hipparcos* parallax were both correct, we should be forced to infer a radius 10 times smaller than for a subgiant and 4 times smaller than for a main-sequence star, but the surface gravity appears inconsistent with such a compact object (since $g \propto M/R^2$). It seems most likely that the *Hipparcos* parallax is simply incorrect, although an examination of

TABLE 3

STELLAR PARAMETERS

Object	$T_{\rm eff}$ (K)	log g	v (km s^{-1})	[Fe/H]
LP 625-44......	5500	2.8	1.6	−2.71
LP 706-7	6000	3.8	1.3	−2.74

the records (D. W. Evans 2001, private communication) revealed no concerns.

An upper limit on the luminosity of LP 706-7 can be inferred via the assumption that it is bound to the Galaxy, the local escape velocity from which appears to be $v_{esc} \sim$ 450–550 km s^{-1} (Ryan & Norris 1991; Allen & Santillan 1991). A luminosity as bright as $M_V = 3.0$ would imply a Galactic rest-frame velocity $v_{RF} = 788$ km s^{-1}, considerably in excess of the escape value, whereas $M_V = 4.0$ would imply $v_{RF} = 464$ km s^{-1}, consistent with the star being bound. This limit on the star's luminosity supports the conclusion from its spectroscopic surface gravity, and from the evolutionary state associated with its effective temperature, that this object has not undergone first dredge-up. This is particularly important for LP 706-7 because radial velocity variations that might be expected for a star with a white dwarf companion have not yet been detected (Norris et al. 1997a). In the following we assume that LP 706-7 has been chemically enriched by a similar process to that experienced by LP 625-44, but the differences between these two stars (LP 706-7 being less evolved and exhibiting no radial velocity variations) should be kept in mind. (Some possible alternative *s*-process sites to AGB stars are also discussed in § 4.1.)

3.2. Pb *Abundance*

In the UV–blue spectrum of the Sun, four Pb I lines have been identified at 3639.5, 3683.4, 3739.9, and 4057.8 Å. Our spectra cover these last two. Youssef & Khalil (1989) tried to analyze Pb in the solar photosphere using their oscillator strengths of these lines. Despite the severe blending with lines of other elements, a Pb abundance log ϵ(Pb) $\sim$ 2.0, consistent with the meteoritic value, was derived from the two lines at 3739.9 and 4057.8 Å. We adopted the line data determined by Youssef & Khalil (1989) in the present analysis. The oscillator strengths of these lines agree well with the recent result by Biémont et al. (2000).

In Figure 2 the synthetic spectra around Pb I λ4057.8 for LP 625-44 and LP 706-7 are shown along with the observed spectra. In this wavelength region the positions of CH lines are identified at 4057.7 and 4058.2 Å, in addition to Mg I λ4057.5. The Pb I λ4057 line is clearly identified in LP 625-44 and also in LP 706-7, though it is much weaker in the latter than in the former.

For comparison, we also show the spectra of HD 140283 and CS 22957-027 in the figure. HD 140283 is a very metal-poor subgiant with similar physical parameters to LP 625-44 and LP 706-7 ($T_{eff} = 5750$ K, log $g = 3.4$, and [Fe/H] $= -2.54$; Ryan, Norris, & Beers 1996), but it exhibits no enhancement of neutron capture elements or of carbon. Since there is no distinct feature at 4057.8 Å in the spectrum of HD 140283, the contamination of metal lines (arising from, e.g., α-elements or iron peak elements), whose abundances in HD 140283 are comparable to those in our carbon-rich objects, is not large at this wavelength in metal-poor subgiants like LP 625-44 and LP 706-7. As a further check on contamination due to CH and CN lines, which might be expected to be a problem in carbon-rich stars, the observed and synthetic spectra of CS 22957-027 are shown in the bottom of Figure 2. Norris, Ryan, & Beers (1997b) showed that this star is a very metal-poor giant ($T_{eff} = 4850$ K, log $g = 1.9$, and [Fe/H] $= -3.38$) with very large excesses of ^{12}C, ^{13}C, and N, but no excess of neutron capture elements. The comparison of this spectrum with those of LP 625-44 and LP 706-7 indicates that the absorption features at 4057.8 Å are not due to the presence of unrecognized CH and CN lines.

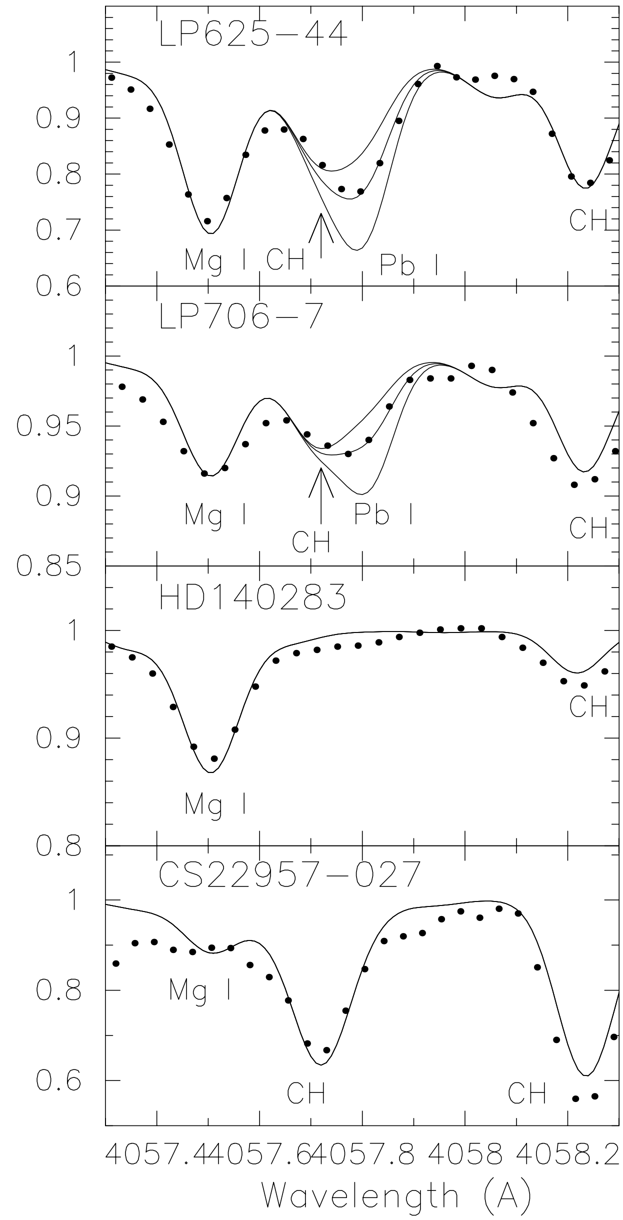

FIG. 2.—Spectra of Pb I λ4057.8 (*filled circles*). The solid lines indicate the synthetic spectra for [Pb/Fe] = 2.25, 2.55, and 2.85 for LP 625-44 and those for [Pb/Fe] = 2.0, 2.3, and 2.6 for LP 706-7. The effects of hyperfine splitting and isotope shifts for the Pb I line are included in the calculation of synthetic spectra. The spectra of HD 140283 and CS 22957-027 are shown for comparison (see text). The synthetic spectra for [Pb/Fe] = 0 are also shown for each star.

The solid lines in Figure 2 are the synthetic spectra calculated using our adopted model atmospheres. The Pb abundances assumed are [Pb/Fe] = 2.25, 2.55, and 2.85 for LP 625-44, [Pb/Fe] = 2.0, 2.3, and 2.6 for LP 706-7, and [Pb/Fe] = 0.0 for the other two stars. The partition function of Pb I derived by Irwin (1981) was used in the analysis. In the calculation of the synthetic spectra, the effect of hyperfine splitting and isotope shifts on the Pb I line is included, whereas the abundance analysis of Paper I used a single-line approximation (the data are given in Appendix A, Table

A6). These changes reduce the Pb abundance for LP 625-44 by 0.1 dex compared to the result in Paper I. The effect of these splittings is much smaller for LP 706-7 because the Pb I line is weaker. Table A6 in Appendix A assumes the solar system isotope ratio for Pb (^{204}Pb:^{206}Pb:^{207}Pb:^{208}Pb = 0.015:0.236:0.226:0.523). For LP 625-44, we also tried the isotope ratio predicted for the *s*-process in AGB stars (Arlandini et al. 1999) (^{204}Pb:^{206}Pb:^{207}Pb:^{208}Pb = 0.04:0.24:0.28:0.44), but we found that the difference from the result derived using the solar system ratio is negligible. We adopted the Pb abundances derived using the solar system Pb isotope ratio and list them in Table 4.

Another Pb I line covered by our blue spectra is Pb I λ3739 (log $gf = -0.12$ and $\chi = 2.66$ eV). However, no distinct absorption feature appears at this wavelength in our spectra. The upper limit on the Pb abundance ([Pb/Fe] < 3.2) derived for this line in LP 625-44 (Paper I) is uninteresting. The same is true in LP 706-7. No additional information could be obtained from the Pb I λ7229 line (log $gf = -1.61$ and $\chi = 2.66$ eV; Biémont et al. 2000), covered by the red spectrum of LP 625-44, because of the weakness of this line.

3.3. *Other Neutron Capture Elements*

Abundances of other neutron capture elements besides Pb are also important to understand nucleosynthesis at low metallicity. As shown by Norris et al. (1997a), the abundances of neutron capture elements in these two stars are basically explained by the predictions of canonical *s*-process nucleosynthesis. We previously reported neutron capture abundances of LP 625-44 in Paper I but have improved them in the present effort by considering hyperfine splitting and isotope shifts for as many lines as possible, and for some elements by studying additional lines. Here we summarize the details of the abundance analysis of neutron capture elements in LP 625-44. We reviewed the spectrum of LP 706-7 used in Norris et al. (1997a) for additional elements but added only Pb. For this reason we used the abundances derived by Norris et al. (1997a) for neutron capture elements (other than Pb) for LP 706-7.

An extensive line list for many neutron capture elements was compiled by Sneden et al. (1996), for their analysis of the *r*-process–enhanced star CS 22892-052. We supplemented their list with many new lines that were detected in LP 625-44 because of its larger excess of neutron capture elements. In Table 2 we list the line data adopted in this work as well as the equivalent widths measured in § 2. Lines included after Paper I was completed are indicated by a footnote. Moreover, we include the effects of hyperfine splitting and isotope shifts to the extent possible for Ce, Pr, Nd, and Sm, in addition to La and Eu, for which Norris et al. (1997a) computed such effects in their subset of lines. In Table 2 the abundances determined by the present analysis and including the effect of splittings [$\delta(\log \epsilon) = \log \epsilon_{\rm singleline} - \log \epsilon_{\rm HFS,IS}$] are given in the fifth and sixth columns, respectively.

Below we describe the line data and provide comments on the abundance analysis for each element. More detailed data on the hyperfine splitting and isotope shifts are given in Appendix A.

Strontium, Yttrium, Zirconium.—The line data listed by Sneden et al. (1996) were employed for the analysis of Sr II and Y II. The *gf*-values measured by Biémont et al. (1981), also used by Sneden et al. (1996), were adopted for Zr II. While the two Sr II lines ($\lambda\lambda$4077.7 and 4215.5) are very strong, another line (λ4161.8) is quite weak. The abundance derived from Sr II λ4161.8 is higher by 0.3 dex than those derived from other strong lines, similar to the results reported by Sneden et al. (1996). We averaged the abundances derived from these three lines.

Barium.—Since the Ba II resonance line at 4554 Å is extremely strong (the equivalent width is 245 mÅ), we excluded this line from the abundance analysis. We used three Ba II lines in the red spectrum because the lines are not so strong as the resonance line and the effect of hyperfine

TABLE 4

[Fe/H] AND RELATIVE ABUNDANCES, [X/Fe]

	LP 625-44				LP 706-7			
ELEMENT	[X/Fe]	log $\epsilon_{\rm el}$	n	σ	[X/Fe]	log $\epsilon_{\rm el}$	n	σ
Fe I ([Fe/H])	−2.71	4.78	34	0.13	−2.74	4.75	74	0.16
Fe II ([Fe/H])......	−2.70	4.79	3	0.18	...	...	...	...
C (CH, C_2).........	2.1	8.0	...	...	2.15	7.96	...	0.23
N (CN)	1.0	6.3	...	...	1.80	7.03	...	0.35
Sr II	1.15	1.37	3	0.16	0.15	0.33	2	0.18
Y II	0.99	0.52	2	0.12	0.25	−0.26	2	0.19
Zr II	1.34	1.25	4	0.12	<1.16	...	1	0.21
Ba II	2.74	2.26	3	0.20	2.01	1.49	4	0.14
La II	2.46	0.98	14	0.13	1.81	0.29	4	0.19
Ce II	2.27	1.20	26	0.12	1.86	0.75	2	0.31
Pr II	2.45	0.58	14	0.12	...	...	...	...
Nd II...............	2.30	1.08	8	0.12	2.01	0.76	2	0.27
Sm II...............	2.21	0.48	23	0.12	<2.21	...	1	0.20
Eu II	1.97	−0.2	2	0.20	1.40	−0.79	1	0.20
Gd II...............	2.31	0.70	6	0.13	...	...	...	...
Dy II...............	1.64	0.1	4	0.2	...	...	...	...
Er II	2.04	0.3	2	0.2	...	...	...	...
Tm II	1.96	−0.6	1	0.2	...	...	...	...
Hf II	2.76	0.8	2	0.2	...	...	...	...
Pb I................	2.55	1.9	1	0.2	2.28	1.6	1	0.2

splitting is small. Norris et al. (1997a) gave the limit on the effect of hyperfine splitting in the λ6496 line as less than 0.02 dex for LP 625-44. We confirmed that the effect is also smaller than 0.02 dex for the $\lambda\lambda$5853 and 6141 lines using the line data provided by McWilliam (1998). For these lines the *gf*-values in Sneden et al. (1996) are adopted.

Lanthanum.—The *gf*-values listed by Sneden et al. (1996) were used for five lines, while the values determined by Bord, Barisciano, & Cowley (1996) were adopted for others. The agreement of *gf*-values between Sneden et al. (1996) and Bord et al. (1996) is fairly good. This element has only one significant isotope (^{139}La). We included the effect of hyperfine splitting for every line, though for most lines the splitting of the upper level is unknown and assumed to be zero (see Appendix A). The $\delta(\log \epsilon)$ values of these lines must be regarded as uncertain and are flagged by a colon in the sixth column of Table 2. Even with this coarse simplification, the effect of the splitting is highly significant for several lines, $\simeq$1.5 dex for $\lambda\lambda$3949, 3988, and 4238. Although we did not include the effect of hyperfine splitting in Paper I, the lines adopted there were quite weak and the effect is not severe; the abundance from our new work is lower by only 0.04 dex, but now it is based on 14 lines, rather than just five lines as in Paper I.

Cerium.—We identified more than 100 Ce II lines in the spectrum of LP 625-44 using the line list of Corliss & Bozman (1962). We selected 26 weak, unblended lines for the abundance analysis. Since there is no reliable source of oscillator strengths for most lines, we scaled the *gf*-values of Corliss & Bozman (1962) to be consistent with those determined by Gratton & Sneden (1994) ($\langle \log gf_{\rm GS94} - \log gf_{\rm CB62} \rangle = 0.23$). Since all Ce isotopes have even-*N* nuclei, most being ^{140}Ce and ^{142}Ce, there is no hyperfine splitting. We have approximated the isotope shifts for the two significant isotopes (see Appendix A) but find that the effect on abundances is quite small ($\leq$0.01 dex) in the weak lines selected in the present analysis. Therefore, the effect was neglected. The limits on $\delta(\log \epsilon)$ shown in Table 2 are nevertheless flagged as uncertain because of the approximate nature of the isotope shift calculation.

Praseodymium.—We adopted the *gf*-values measured by Goly et al. (1991) for six lines. For other lines, Corliss & Bozman (1962) values scaled to Goly et al. (1991) are used ($\langle \log gf_{\rm Goly91} - \log gf_{\rm CB62} \rangle = 0.60$). Since there is only one stable isotope ^{141}Pr, there is no isotope shift, but hyperfine splitting for this odd-*N* nucleus is sometimes significant, giving $\delta(\log \epsilon)$ values up to 0.64.

Neodymium.—Following Sneden et al. (1996), we adopted the oscillator strength determined by Maier & Whaling (1977) and corrected the values by Ward et al. (1985). We reselected the lines for which reliable *gf*-values exist. Since we have no information on hyperfine splitting, we included only the isotope shift, using the solar system isotope ratios. As odd-*N* nuclei account for only 20% of the solar system Nd isotopes, hyperfine effects should be small. The maximum effect computed, 0.15 dex, appears for the $\lambda\lambda$4061 and 4462 lines.

Samarium.—We adopted the *gf*-values provided by Biémont et al. (1989) for six lines and the Corliss & Bozman (1962) values scaled to Biémont et al. (1989) for the other 17 lines ($\langle \log gf_{\rm B89} - \log gf_{\rm CB62} \rangle = 0.49$). There are seven main isotopes for Sm. While we neglected hyperfine splitting as a result of insufficient information, we included the isotope shifts and assumed solar system isotope ratios. As given in Table 2, the effect of the isotopic shift is small ($\leq$0.08); one of the reasons is that the lines selected in our analysis are quite weak. Therefore, this effect should be negligible even if the isotope ratios are different from the solar system values.

Europium.—We adopted the *gf*-values determined by Biémont et al. (1982). The λ4205.5 line, which is frequently used for abundance analysis, was excluded because of severe blending with CH molecular lines. The λ3930 line was detected but is strongly blended with an Fe I line; we also excluded this line. The line strengths and shapes for Eu II $\lambda\lambda$3819 and 4129 are strongly dependent on the isotope ratio (Eu^{151}:Eu^{153}), but the appropriate value is unknown. The solar system isotope ratio is Eu^{151}:Eu^{153} = 0.49:0.51, but most solar system Eu originates in the *r*-process, whereas LP 625-44 and LP 706-7 are *s*-process dominated. Käppeler et al. (1989) derived the isotope ratio of the *s*-process main component as Eu^{151}:Eu^{153} = 0.02:0.98, very different from the solar system ratio, but the value predicted by a recent calculation of the *s*-process in AGB stars (Arlandini et al. 1999) is Eu^{151}:Eu^{153} = 0.54:0.46, similar to the solar system one. Thus, it is difficult at present to know the appropriate isotope ratio for the abundance analysis of Eu II $\lambda\lambda$3819 and 4129 lines. For this reason we used only two lines (Eu II $\lambda\lambda$3907 and 4522) for which the effects of hyperfine splitting and isotope shift are much smaller (see Table 2).

Gadolinium.—For the λ4085.5 line, the transition probability determined by Bergström et al. (1988) was adopted. For other lines we adopted *gf*-values in Corliss & Bozman (1962) with no correction because Bergström et al. (1988) reported that there is no systematic discrepancy between their results and those of Corliss & Bozman (1962). Insufficient data were found to permit calculations of isotopic shifts or of hyperfine splitting for the 30% of odd-*N* isotopes.

Dysprosium.—Transition probabilities of Dy II lines were determined by Kusz (1992). Since we found no useful data on hyperfine splitting for Dy II lines, we neglected it, but the effect should be small because the lines used for abundance analysis are quite weak. Spectrum synthesis was applied because the lines have some blending with other elements.

Erbium, Thulium, Hafnium.—For these three elements, the line data compiled by Sneden et al. (1996) were used. The abundances were determined by spectrum synthesis with a careful check of line blending.

A standard abundance analysis, based on the measured equivalent widths, was applied to unblended lines, for which the equivalent widths are listed without a footnote in Table 2. The standard analysis was also applied to lines of La, Ce, Pr, Nd, and Sm, which are affected by hyperfine splitting and isotope shifts. In those cases, however, equivalent widths were computed by integrating the synthetic spectrum of multicomponent lines and then comparing with the observed ones. As for the Pb I line, we have confirmed that there are no distinct features of CH and CN at these wavelengths in the spectrum of CS 22957-027, which has strong molecular features but almost no absorption by neutron capture elements. Spectrum synthesis was applied in the case of lines that are blended with lines of other elements or molecules. In Figure 3 examples of the comparison between observed and synthetic spectra for Dy II, Er II, and Hf II are shown.

The abundances derived for LP 625-44 are given in

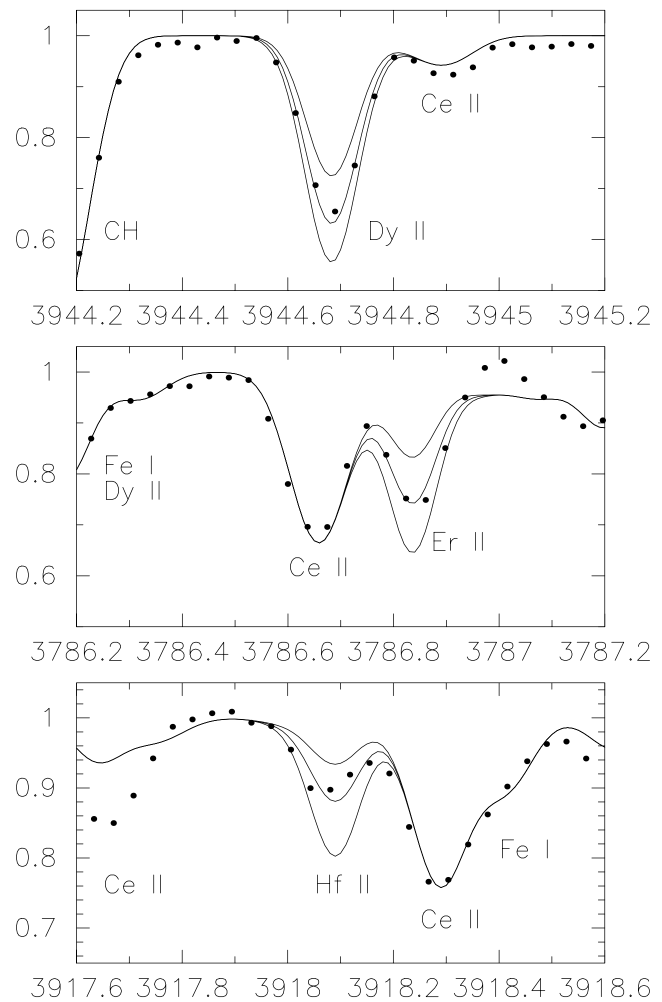

FIG. 3.—Comparison between the observed spectrum of LP 625-44 and synthetic spectra for [Dy/Fe] = 1.7 (*top*), [Er/Fe] = 2.0 (*middle*), and [Hf/Fe] = 2.6 (*bottom*). Two alternative synthetic spectra for Δ[X/Fe] = ± 0.3 are also shown in each panel.

Table 4. The errors were estimated following the treatment of Ryan et al. (1996). The errors from the uncertainties of the atmospheric parameters were evaluated by adding in quadrature the individual errors corresponding to $\Delta T_{\rm eff} = 100$ K, $\Delta \log g = 0.3$, and $\Delta v = 0.5$ km s^{-1}. The internal errors were estimated by assuming the random error in the measurement of equivalent widths to be 4 mÅ (and 6 mÅ for Ba II in the red region), as measured in Paper I, and taking the random error associated with uncertain *gf* values to be 0.1 dex. For convenience the abundances of LP 706-7 determined by Norris et al. (1997a) are also listed in Table 4 along with the Pb abundance derived in the previous section.

3.4. *Carbon and Nitrogen*

Carbon, nitrogen, and oxygen abundances, and their isotope ratios, are quite important for understanding the processes that take place in the interior of AGB stars. The excess carbon in the outer atmospheres of AGB stars is recognized as a result of the triple-α process in the thermal pulse and mixing during the third dredge-up. Nitrogen is synthesized through the CN(O) cycle, while the carbon abundance decreases by this process. The carbon isotope ratio (C^{12}/C^{13} ratio) also usually decreases toward the equilibrium value ~ 3. In the present work, the carbon and nitrogen abundances were redetermined for LP 625-44 using the new, higher quality spectrum. Moreover, the carbon isotope ratio ($^{12}C/^{13}C$) was also determined from the ^{13}CH lines in the spectrum of LP 625-44.

The carbon and nitrogen abundances were determined by the molecular features of CH at 4323 Å and CN at 3883 Å as in Norris et al. (1997a). The oxygen abundance assumed in the analysis is [O/Fe] = 1.0. The derived carbon and nitrogen abundances are not sensitive to this assumption in very carbon-rich subgiants; we tested the range 0.0 < [O/Fe] < 1.5 but found that the effect on abundance determination for carbon and nitrogen is negligible. One reason for this result is that the temperature of LP 625-44 is high, and the fraction of carbon bound in the CO molecule is quite small. Another is that the oxygen abundance assumed here [$\log \epsilon$(O) < 7.67] is much smaller than the carbon abundance [$\log \epsilon$(C) $\sim$ 8.0], and the influence of the assumed oxygen abundance on determination of carbon abundance is smaller than that of the oxygen-rich case. The result is given in Table 4. The carbon abundance derived here agrees with that by Norris et al. (1997a) within the uncertainty. However, the nitrogen abundance reported here is lower by 0.65 dex than that of Norris et al. (1997a). One reason is the higher carbon abundance (by 0.15 dex) inferred here, which increases the formation of CN molecules. This explains 0.15 dex of the discrepancy. Another reason is that the dissociation energy of the CN molecule adopted in this analysis (7.85 eV; Aoki & Tsuji 1997) is higher by 0.09 eV than that in Norris et al. (1997a) and likewise increases CN formation. As a result, the derived nitrogen abundance is lower by 0.10 dex than that calculated assuming E_0^0(CN) = 7.66 eV. The oscillator strengths of CN lines are also uncertain, as discussed in Norris et al. (1997a). In the present analysis, the oscillator strengths determined by Bauschlicher, Langhoff, & Taylor (1988) were adopted. Because of these uncertainties in the analysis, further investigation of other features, such as the NH λ3360 lines, is indispensable for a detailed discussion of nitrogen abundance.

The carbon isotope ratio of LP 625-44 was determined using the ^{13}CH features around 4200 Å. The synthetic spectra for $^{12}C/^{13}C$ = 10, 20, and 40, fitted to the observed spectrum around 4210–4225 Å, are shown in Figure 4. In this wavelength region, six "almost clean" ^{13}CH lines are identified. The line positions were calculated using the molecular constants derived by Zachwieja (1995) and Zachwieja (1997) for ^{12}CH and ^{13}CH ($A^2\Delta$–$X^2\Pi$ system), respectively. In the figure we also show the corresponding ^{12}CH lines, which lie about 0.35 Å blueward of the ^{13}CH lines. From the analysis, a ratio $^{12}C/^{13}C \sim 20$ was derived for LP 625-44. The spectrum of LP 706-7 was reviewed, but CH features are much weaker than those in the LP 625-44 spectrum, and no useful ^{13}CH line was found. A higher quality spectrum is required for the determination of the carbon isotope ratio in LP 706-7.

4. DISCUSSION

4.1. *The Overabundance of Neutron Capture Elements*

In Figure 5 the relative abundances of neutron capture elements ([X/H]) are shown as a function of atomic number for the two stars. The horizontal lines indicate the values of [Fe/H].

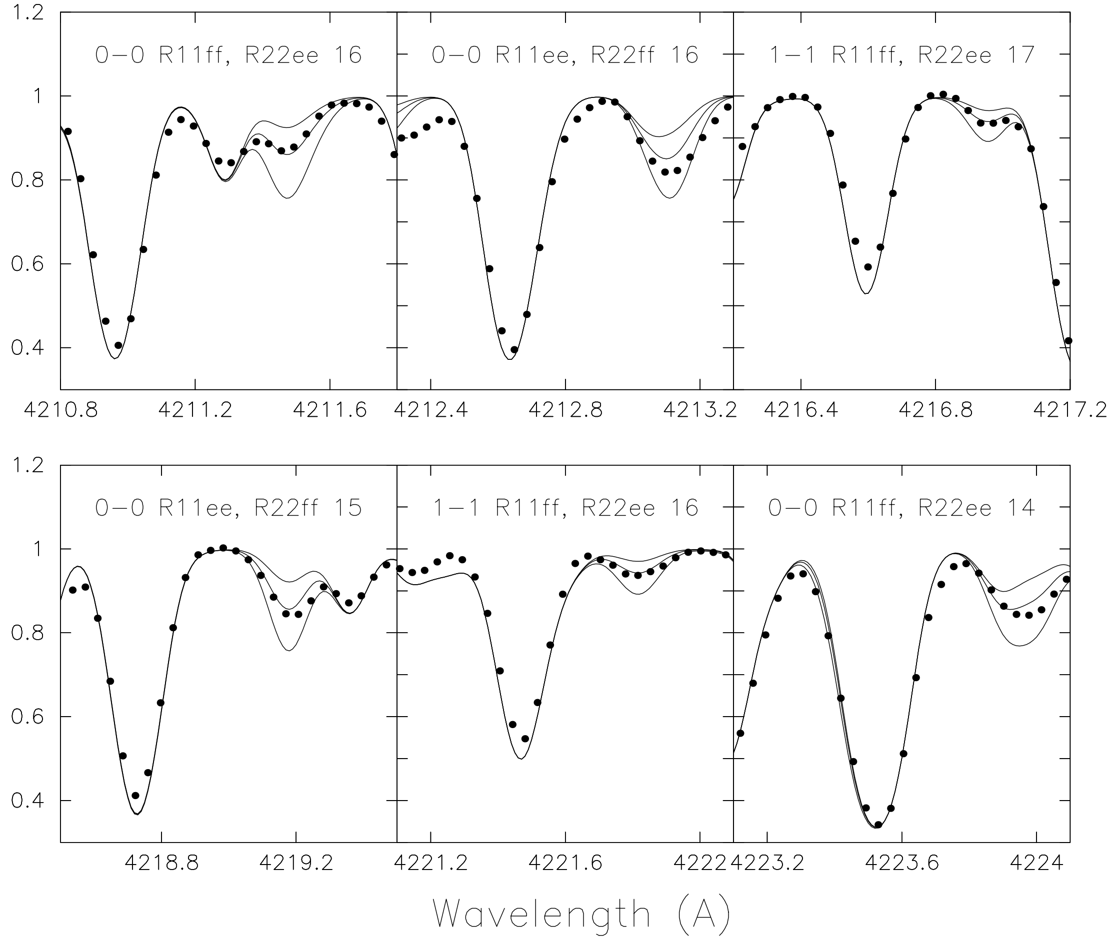

FIG. 4.—Comparison between the observed spectrum of LP 625-44 and synthetic spectra for $C^{12}/C^{13} = 10$, 20, and 40 for six ^{13}CH lines. The line identification is given in each panel. We also show the corresponding ^{12}CH lines, which lie about 0.35 Å blueward of the ^{13}CH lines.

Abundance studies of metal-poor stars with [Fe/H] < -2.5 have revealed that the contribution of the *s*-process to the abundance of neutron capture elements is small at this level of enrichment. This is probably because the *r*-process elements originate from nucleosynthesis in massive stars, which evolve quickly ($\sim 10^7$ yr) and eject heavy elements into the interstellar medium. There are almost no *s*-process elements formed in the early Galaxy until the average metallicity [Fe/H] $\gtrsim -2$ (Mathews, Bazan, & Cowan 1992). However, we found strong excesses of neutron capture elements in the two metal-deficient stars LP 625-44 and LP 706-7 with [Fe/H] $= -2.7$ and -2.74, respectively, which are interpreted as the result of *s*-process nucleosynthesis from a single site. Namely, the abundant material polluted by *s*-process nucleosynthesis dominates over the original surface abundances of neutron capture elements. For instance, the Ba abundance in these two stars is a factor of several hundred times higher than the general trend of model predictions at [Fe/H] $= -2.7$. Even the abundance of Eu, which is usually interpreted as a signature of the *r*-process, but should also be produced by the *s*-process as well, is enhanced by more than a factor of 10 in these two stars. Therefore, the neutron capture elements in these two stars should present almost pure products of *s*-process nucleosynthesis at low metallicity. The exceptions to this are the abundances of Sr and Y in LP 706-7, which show no distinct excess. Therefore, the contribution of the *s*-process to these two elements may not be significant for this star.

In the following discussion we analyze the abundance ratios of neutron capture elements in these two stars. We treat them as having been produced in a single *s*-process site and seek to understand the characteristics of a process that best explains the abundances of LP 625-44 and LP 706-7.

Our discussion below is not based on any specific stellar model, but interest is focused mostly on the nucleosynthesis process in AGB stars (§§ 1 and 3.1). For completeness, we note here some possible alternative *s*-process to AGB stars. The *s*-process nucleosynthesis in helium core burning massive stars has been studied by The, El Eid, & Meyer (2000) and Rayet & Hashimoto (2000) using updated neutron capture cross sections. The nucleosynthesis products in these models, however, have their abundance peak centered on the lighter elements ($Z \lesssim 90$) for any parameter choice; furthermore, massive stars are not appropriate as the *s*-process site to explain our two stars. Schlattl et al. (2001) pointed out a possibility of *s*-process nucleosynthesis during the phase of helium core flash in low-mass, extremely metal-poor stars based on their model calculations for the metal-free case. This kind of study can be a useful approach to understand the abundances of some carbon-rich and *s*-process–rich stars and should be given further attention in the future. An interesting recent obser-

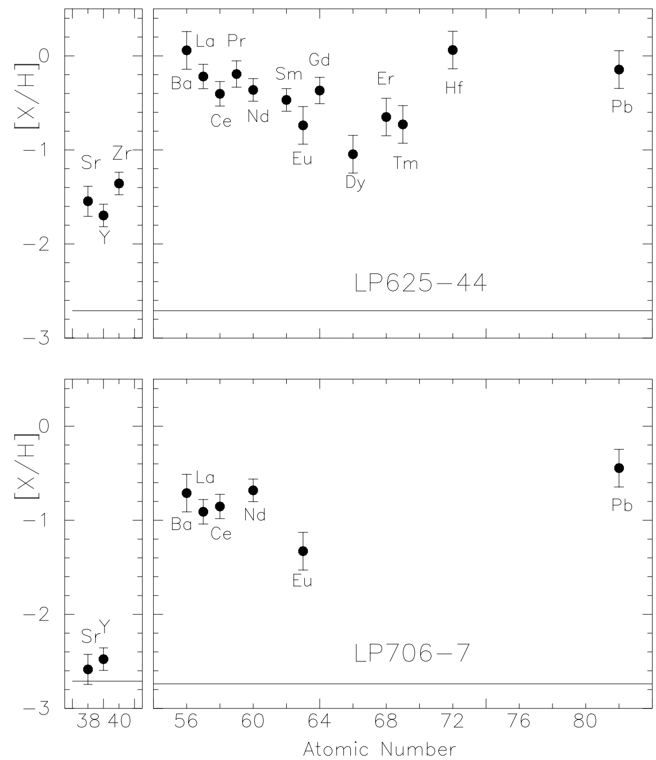

FIG. 5.—Abundance ratios ([X/H]) as a function of atomic number for LP 625-44 (*top*) and for LP 706-7 (*bottom*). The horizontal lines indicate the values of [Fe/H].

vational result has been reported by Preston & Sneden (2001). These authors conducted a long-term radial velocity monitoring program for carbon-enhanced metal-poor stars and found that none of the three carbon-rich subgiant CH stars they studied exhibited velocity variations over an 8 yr period. They conclude that these stars are likely to have undergone an enhanced mixing event at the end of their giant branch evolution that puts these stars at the base of the subgiant branch again, as a result of increased hydrogen mixing into their cores. One of our stars, LP 625-44, clearly shows a variation of radial velocity (Aoki et al. 2000) and may not be similar to the stars in Preston & Sneden (2001). However, there is no evidence of binarity for the other, LP 706-7 (Norris et al. 1997a). This indicates that the suggestion by Preston & Sneden (2001) might indeed apply to this star, and further investigation of abundances and binarity for these (and other) subgiants, as well as the theoretical studies, is desirable.

4.2. *Physical Conditions for s-Process Nucleosynthesis*

There have been many theoretical studies of *s*-process nucleosynthesis in low- to intermediate-mass AGB stars. The best candidate reactions for the neutron source are either the $^{13}C(\alpha, n)^{16}O$ (Cameron 1955; Reeves 1966; Mathews & Ward 1985) or $^{22}Ne(\alpha, n)^{25}Mg$ (Cameron 1960). In order for the former reaction to occur in AGB stars, sufficient protons must be injected into the ^{12}C-rich layer, which lies below the hydrogen-rich envelope in AGB stars. ^{13}C is then produced in the CN cycle

$$^{12}C(p, \gamma)^{13}N(e^+\nu)^{13}C , \tag{1}$$

and ^{22}Ne is produced (after the accumulation of ^{14}N from the CNO cycle) via the reaction sequence

$$^{14}N(\alpha, \gamma)^{18}F(e^+\nu)^{18}O(\alpha, \gamma)^{22}Ne . \tag{2}$$

Unfortunately, however, the precise mechanism for chemical mixing of protons from the hydrogen-rich envelope into the ^{12}C-rich layer is still unknown, even for stars with solar metallicity, despite several theoretical efforts (Herwig et al. 1997; Langer et al. 1999). This makes it even harder to understand the peculiar abundance pattern of the *s*-process elements found in carbon-rich, metal-deficient stars such as LP 625-44 and LP 706-7. Gallino et al. (1998) and Busso et al. (1999) have recently proposed an *s*-process model for metal-deficient stars that may proceed in the so-called ^{13}C pocket (Straniero et al. 1995) during the relatively long interpulse period $\sim$10,000 yr. Since ^{13}C is too scarce in ordinary hydrogen-burning ashes, they have to introduce a freely adjustable parameter to fix the total amount of ^{13}C. This provides enough neutrons so that the model calculation explains the *s*-process abundance distribution for stars with $-2 \leq$ [Fe/H] ≤ 0.

As an alternative, we have studied what physical conditions are necessary to reproduce the observed *s*-process abundance profile of LP 625-44 and LP 706-7 without adopting any specific stellar model. For this purpose, we have applied the parametric model of Howard et al. (1986), with many of the neutron capture rates updated (Bao et al. 2000). There are four parameters in this model, only three of which are independent. They are the neutron irradiation time, Δt, the neutron number density, N_n, the temperature, T_9 (in units of 10^9 K), at the onset of the *s*-process, and the overlap factor, r, which is the fraction of material that remains to experience subsequent neutron exposures. These quantities can be combined to give the neutron exposure per thermal pulse, $\tau = N_n v_T \Delta t$, where v_T is the average thermal velocity of neutrons at T_9. In the case of multiple subsequent exposures the mean neutron exposure is given by $\tau_0 = -\tau/\ln r$. The final abundance distributions depend only upon the neutron exposure, as long as the neutron density is not so high that significant branchings occur along the *s*-process path. The temperature is fixed at a reasonable value for the $^{13}C(\alpha, n)^{16}O$ reaction, $T_9 = 0.1$, for these studies. We carried out *s*-process nucleosynthesis calculations to fit individually the abundance profile observed in LP 625-44 and LP 706-7, in order to look for the minimum χ^2 in the three-parameter space formed by Δt, N_n, and r. The adopted initial abundances of seed nuclei lighter than the iron peak elements were taken to be the solar system abundances, scaled to [Fe/H] $= -2.7$. For the other heavier nuclei we use solar system *r*-process abundances (Arlandini et al. 1999), normalized to that expected for a star with [Fe/H] $= -2.7$. This is a natural assumption because the neutron capture element component of the interstellar gas that formed very metal-deficient stars is expected to consist of mostly pure *r*-process elements, as proposed by Truran (1981) and seen in various halo star observations (Spite & Spite 1978; Gilroy et al. 1988).

Figures 6 and 7 show our calculated best-fit model for our two metal-deficient stars. The parameters deduced for LP 625-44 are $N_n = 10^7$ cm^{-3}, $r = 0.1$, and $\Delta t \approx 1.7 \times 10^4$ yr, which corresponds to a neutron exposure per pulse of $\tau = 0.71 \pm 0.08$ (1 σ) mbarn^{-1} and a mean neutron exposure $\tau_0 = (0.58 \pm 0.06)(T_9/0.348)^{1/2}$ mbarn^{-1}. We comment below on the permissible range of N_n and uncertainty of the adopted parameters. The derived parameters for the other

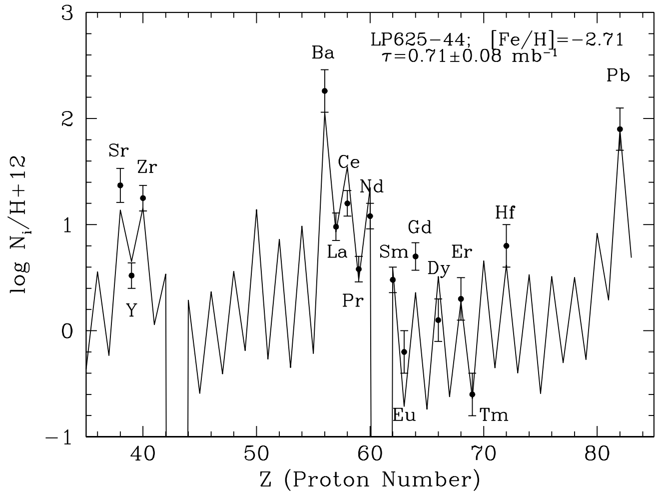

FIG. 6.—Best fit to observational results of very metal-deficient star LP 625-44, using the *s*-process nucleosynthesis model with neutron exposure $\tau = 0.71 \pm 0.08$ mbarn^{-1}. [*See the electronic edition of the Journal for a color version of this figure.*]

metal-deficient star, LP 706-7, are $\Delta t \approx 1.9 \times 10^4$ yr with the same N_n and r, which corresponds to a neutron exposure per pulse of $\tau = 0.80 \pm 0.09$ ($1\ \sigma$) mbarn^{-1} and a mean neutron exposure $\tau_0 = (0.65 \pm 0.07)(T_9/0.348)^{1/2}$ mbarn^{-1}. The relative abundance ratios for Pb/Sr and Ba/Sr in LP 706-7 are slightly larger than those in LP 625-44. This small difference is accounted for by a slight increase of neutron exposure τ. It is noteworthy, however, that these values for the mean exposure are significantly larger than those that best fit solar system material, $\tau_0 = (0.30 \pm 0.01)(T_9/0.348)^{1/2}$ (Käppeler et al. 1989). Gallino et al. (1998) found a neutron exposure $\tau_{max} \approx 0.4$–0.5 in their ^{13}C pocket model for the solar system *s*-process abundances. Applying this to metal-deficient stars, Busso et al. (1999) predicted an extremely

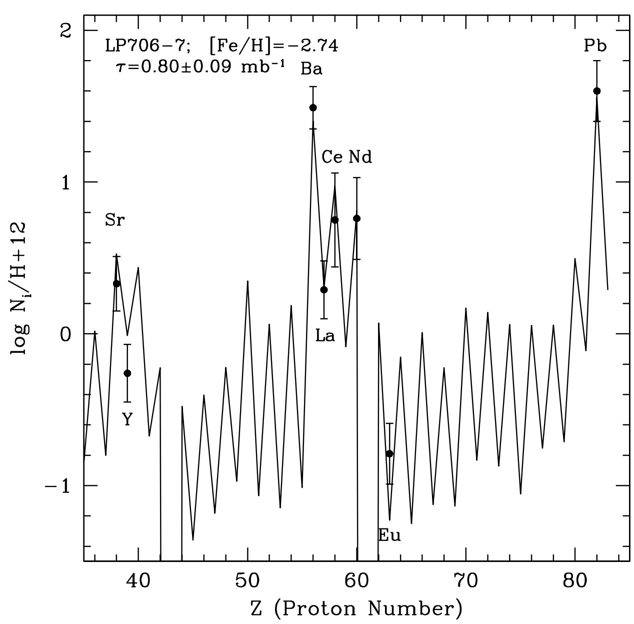

FIG. 7.—Best fit to observational results for the very metal-deficient star LP 706-7, using the *s*-process nucleosynthesis model with neutron exposure $\tau = 0.80 \pm 0.09$ mbarn^{-1}. [*See the electronic edition of the Journal for a color version of this figure.*]

enhanced Pb abundance, Pb/Ba > 100, much larger than the observed value, Pb/Ba ~ 1, for LP 625-44 and LP 706-7 (we define $A/B = N_A/N_B$ and N_A the number density of nucleus A).

We found in our nucleosynthesis calculations that, as long as the same neutron exposure is adopted, the abundance patterns of LP 625-44 and LP 706-7 are reproduced with equivalent reduced χ^2 values, even in extreme conditions of very high neutron density, $N_n \gtrsim 10^{11}$ cm^{-3}. These parameter values simulate, more or less, the *s*-process conditions expected during the thermal pulse phase (Iben 1977). Hence, although we can constrain the neutron exposure quite well (for this class of models), we cannot distinguish easily the neutron density for the *s*-process based solely upon these data.

4.3. *Lead Production by Large Neutron Exposure*

The abundance analyses shown in Figures 6 and 7 reveal three prominent peaks at Sr-Zr, Ba, and Pb in the *s*-process element profile, corresponding to closed neutron shells with $N = 50$, 82, and 126. We therefore discuss the dependence of the *s*-process yields of Pb/Ba and Ba/Sr on the neutron exposure τ. These ratios are useful as a means to constrain the physical conditions of the *s*-process.

An illustration of the evidence for a large-exposure, multipulse model is given in Figure 8. This figure shows the calculated elemental ratios log (Pb/Ba) and log (Ba/Sr) as a function of the exposure per pulse τ in a model with $r = 0.1$. These are compared with the observed ratios from LP 625-44. There is only a narrow region of overlap, $\tau = 0.71 \pm 0.08$ ($1\ \sigma$) mbarn^{-1}, in which both the observed large Ba/Sr ratio and moderate Pb/Ba ratio can be

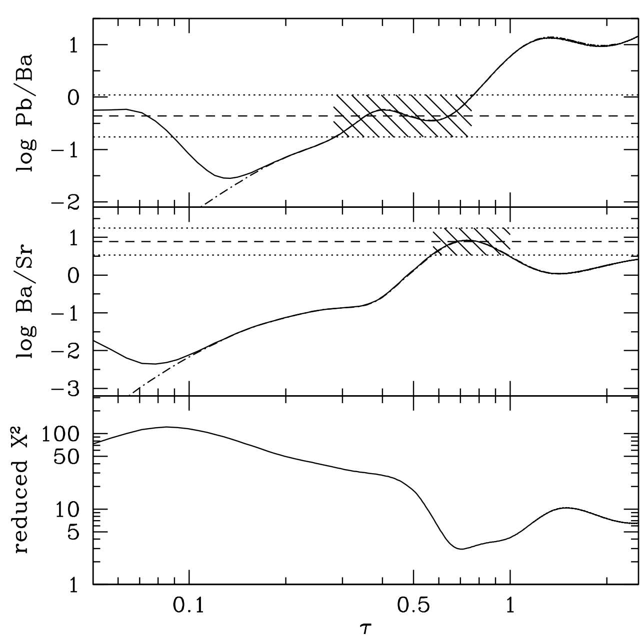

FIG. 8.—Abundance ratios log (Pb/Ba) (*top*), log (Ba/Sr) (*middle*), and reduced χ^2 (*bottom*), as a function of the neutron exposure per pulse, τ, in a model with overlap factor $r = 0.1$. Solid curves refer to the theoretical results, and dashed horizontal lines refer to the observational results with errors expressed by dotted lines. Dot-dashed curves refer to the theoretical results calculated without *r*-process elements and using elements lighter than Fe as seed nuclei. See text for more details. The shaded area illustrates the allowed region for the theoretical model. [*See the electronic edition of the Journal for a color version of this figure.*]

accounted for. The bottom panel displays the reduced χ^2 value, which is calculated in our models with all detected elemental abundances being taken into account. There is a deep minimum, with $\chi^2 \approx 3$, at $\tau = 0.71$ mbarn^{-1} with 1 σ error bar ± 0.08 mbarn^{-1}. There is another shallow minimum, around $\tau \approx 2.3$ mbarn^{-1}, for which the Ba/Sr ratio is close to the observed range. However, this parameter is excluded because τ is so large that the predicted Pb abundance as well as the Pb/Ba ratio are beyond the acceptable observed range (see Fig. 8, *top panel*).

The main features of this figure can be understood qualitatively. For moderate neutron exposure, $\tau \approx 0.1$–0.7 mbarn^{-1} [$\tau_0 \approx (0.08$–$0.6)(T_9/0.348)^{1/2}$ mbarn^{-1}], the product of cross section times abundance for the s-process, $\sigma_A N_A$, can be written (Mathews & Ward 1985; Käppeler et al. 1989)

$$\sigma_A N_A = \frac{\sigma_{A-1} N_{A-1}}{1 + 1/\tau_0 \sigma_A}, \quad (3)$$

where σ_A is the Maxwellian-averaged neutron capture cross section for nucleus A. This product of $\sigma_A N_A$ versus A exhibits a characteristic steplike function in which regions of constant $\sigma_A N_A$ make sudden drops at neutron closed-shell nuclei ^{88}Sr, ^{138}Ba, and ^{208}Pb. After the drop, the curve is again roughly constant. Hence, we can write the following approximate relations for ^{88}Sr, ^{138}Ba, and ^{208}Pb:

$$\sigma_{89} N_{89} = \frac{\sigma_{88} N_{88}}{1 + 1/\tau_0 \sigma_{89}} \approx \sigma_{137} N_{137}, \quad (4)$$

$$\sigma_{138} N_{138} = \frac{\sigma_{137} N_{137}}{1 + 1/\tau_0 \sigma_{138}}. \quad (5)$$

From these we deduce

$$\sigma_{138} N_{138} = \frac{\sigma_{88} N_{88}}{(1 + 1/\tau_0 \sigma_{89})(1 + 1/\tau_0 \sigma_{138})}, \quad (6)$$

for which

$$\frac{N_{\rm Ba}}{N_{\rm Sr}} \approx \frac{\tau_0^2 \sigma_{88} \sigma_{89}}{(1 + \tau_0 \sigma_{89})(1 + \tau_0 \sigma_{138})}. \quad (7)$$

Similarly, for Pb/Ba we have

$$\frac{N_{\rm Pb}}{N_{\rm Ba}} \approx \frac{\tau_0^2 \sigma_{138} \sigma_{139}}{(1 + \tau_0 \sigma_{139})(1 + \tau_0 \sigma_{208})}. \quad (8)$$

Equations (7) and (8) show the basic behavior of a roughly quadratic increase in Ba/Sr and Pb/Ba $\propto \tau_0^2 \propto \tau^2$ displayed in Figure 8. This relation breaks down as $\tau_0 \sigma_A$ approaches unity. For larger exposures, the conditions $\sigma_{138} \gg 1/\tau_0$ and $\sigma_{208} \gg 1/\tau_0$ can be applied to equations (7) and (8). The abundance ratios then asymptotically reach nearly constant values, $N_{\rm Ba}/N_{\rm Sr} \approx \sigma_{88}/\sigma_{138} \approx 10^{0.3}$ and $N_{\rm Pb}/N_{\rm Ba} \approx \sigma_{138}/\sigma_{208} \approx 10^{0.98}$.

The deviation of these ratios from equation (7) to equation (8) is mostly due to the fact that the single-step function approximation breaks down. We can explain at least what kind of effect might cause the deviation. At lower neutron exposure, $\tau \lesssim 0.1$ mbarn^{-1}, the increase in both of the ratios Pb/Ba and Ba/Sr is due to the s-process from seed r-process elements. Since the neutron exposure is too small to affect the s-process from iron peak elements, only a weak s-process operates on seeds from the nearby abundance peaks of the r-process elements. In order to verify this fact quantitatively, we have run our s-process code without the introduction of seed r-process elements. The result is shown by the dot-dashed curve in Figure 8. In this case even the weak s-process mentioned above does not operate at low neutron exposure, $\tau \lesssim 0.1$ mbarn^{-1}, so that both the Pb/Ba and Ba/Sr ratios decrease monotonically as τ decreases. Likewise, at intermediate neutron exposures, $0.1 \lesssim \tau \lesssim 0.7$ mbarn^{-1}, the main s-process operates on the very abundant iron peak elements, as we have already discussed in this section. As the neutron exposure increases further, $\tau \gtrsim 0.7$ mbarn^{-1}, the s-process starts even from the Ne-Si seed abundance peaks that we included in the present calculations. More Ba than Pb and more Sr than Ba are produced from these low-mass seed nuclei, thus regulating the abundance ratios Pb/Ba and Ba/Sr from monotonic growth at $\tau \gtrsim 0.7$ mbarn^{-1}. It is interesting to note in Figure 8 that the structure seen in the ratio Ba/Sr is shifted toward higher neutron exposure in the ratio Pb/Ba, by a factor $\sim$1.5–2.0. This is a natural consequence of the fact that the s-process produces heavy nuclei from lighter seed nuclei. The efficiency of this is proportional to the neutron exposure.

4.4. *Single Pulse or Multipulse? A New s-Process Paradigm*

We have extensively explored the convergence of the abundance distribution of s-process elements through recurrent neutron exposures. Almost all elements, except for Pb, were found to be made in the first neutron exposure. Even the lead abundance converges after about three recurrent neutron exposures. This is consistent with the small overlap factor, $r \approx 0.1$, deduced in our best-fit model. Figure 9 shows the calculated elemental ratios, log (Pb/Ba) and log (Ba/Sr), and reduced χ^2, as a function of the overlap factor, r, with fixed neutron exposure $\tau = 0.71$ for LP 625-44. The observed Pb/Ba ratio is reproduced in the few-pulse model only for a small overlap factor, $r \lesssim 0.2$, while the Ba/Sr ratio is rather insensitive to r and allows for a wider range, $r \lesssim 0.65$. The Pb abundance is so sensitive to r that large r-values ($0.2 \lesssim r$) are almost entirely excluded, as

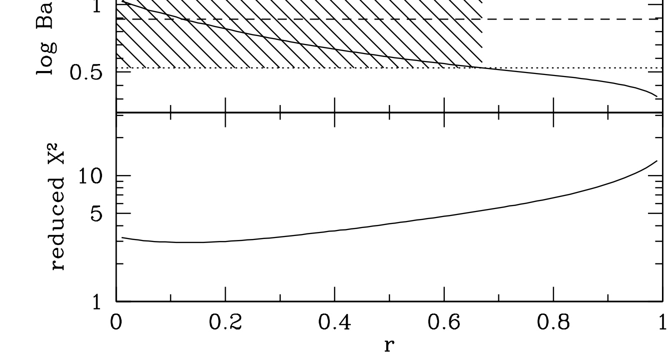

FIG. 9.—Same as those in Fig. 8, but as a function of the overlap factor r. [*See the electronic edition of the Journal for a color version of this figure.*]

shown in the top panel of Figure 9. This is a characteristic feature of the *s*-process pattern observed in LP 625-44 and LP 706-7.

Gallino et al. (1998) have found an overlap factor of $r = 0.4$–0.7 in their standard evolution model of low-mass ($3\ M_{\odot}$) AGB stars at solar metallicity. Theoretical estimates of *r* were reported by Iben (1977) for intermediate-mass ($7\ M_{\odot}$) AGB stars, taking into account the core mass dependence. Howard et al. (1986) used $r = 0.285$ in their *s*-process calculations with a constant neutron density, adopting a $1.16\ M_{\odot}$ CO core model. They found that the *s*-process abundances converge after six to eight pulses. These *r*-values are based upon AGB stars with solar metallicity and are very different from our value $r \approx 0.1$, found for the best fit to metal-deficient AGB stars that produced the abundance patterns of LP 625-44 and LP 706-7.

In an *s*-process scenario that invokes radiative ^{13}C burning (i.e., the ^{13}C pocket model), a small $r \sim 0.1$ may be realized if the third dredge-up is deep enough for the *s*-processed material to be diluted by extensive admixture of unprocessed material. Once this happens, no matter how many pulses may follow, the observed abundance profile of LP 625-44 and LP 706-7 may be reproduced in the first few interpulses, as we demonstrated in the present calculations.

Another possibility is that the *s*-process material in metal-deficient AGB stars has experienced only a few neutron exposures in the convective He-burning shell. This is consistent with a newly proposed mechanism for the *s*-process in metal-deficient AGB stars (Fujimoto, Ikeda, & Iben 2000). These authors proposed a scenario in which the convective shell triggered by the thermal runaway develops inside the helium layer and penetrates into the hydrogen-rich envelope. This carries protons to the He- and ^{12}C-rich layers. Once this occurs, ^{12}C captures proton to synthesize ^{13}C and other neutron source nuclei. The thermal runaway continues to heat material in the thermal pulse so that neutrons produced by the $^{22}Ne(\alpha, n)^{25}Mg$ reaction as well as the $^{13}C(\alpha, n)^{16}O$ reaction may contribute. Detailed stellar evolution calculations are therefore highly desired, in order to clarify which site is the most likely to dominate the *s*-process in metal-deficient AGB stars: interpulse (Gallino et al. 1998) or thermal pulse (Fujimoto et al. 2000; N. Iwamoto et al. 2001, in preparation).

It is worth commenting on the contrasting behavior of Pb/Ba and Ba/Sr as a function of overlap factor *r* seen in Figure 9. Whereas [Pb/Ba] increases with higher overlap, Ba/Sr decreases. The former behavior may be understood as the achievement of a higher number of captured neutrons per seed when the overlap factor is higher because additional neutrons will be captured during repeat processing. This pushes the distribution of *s*-process nuclei to higher atomic numbers, especially for Pb, since it is in one sense the end point of the *s*-process production line. Ba/Sr must also increase in response to this, but for Sr an additional factor comes into play, the enhanced production of new *s*-process nuclei just beyond the iron peak due to great abundance of iron peak seeds. This source of Sr more than makes up for the processing of Sr toward Ba, with the net effect that Ba/Sr decreases with increasing overlap factor, in contrast to the behavior of Pb/Ba.

4.5. *Origin of Lead*

The enrichment of Pb is one of the long-standing problems in the chemical evolution of the Galaxy. Most ($\sim 80\%$) of the Pb in the solar system is believed to be produced by *s*-process nucleosynthesis. However, the Pb abundance in the solar system cannot be explained by the main *s*-process component alone. A strong component, with a much higher neutron exposure, has therefore been postulated (e.g., Käppeler et al. 1989).

Low-mass, metal-poor AGB stars have been proposed as a site for *s*-process nucleosynthesis of Pb (Gallino et al. 1998). Based on the stellar yields and on a model of the Galactic chemical evolution, Travaglio et al. (2001) discussed the origin and the enrichment history of Pb in the Galaxy. They concluded that low-metallicity, low-mass AGB stars are the main contributors of Pb to the Galaxy.

The yields of the *s*-process elements, including Pb, calculated by the Torino models are dependent on the assumed amount of ^{13}C (the neutron source) in the He intershell in which *s*-process nucleosynthesis occurs. However, the amount of ^{13}C cannot, at present, be determined theoretically and is constrained only by observations of the abundances of *s*-process elements. Theoretical arguments (Gallino et al. 1998) and observational constraints for moderately metal-poor stars ([Fe/H] ~ -1) (Busso et al. 1999) indicate that no single value suffices, i.e., a range of ^{13}C source material is required. Consequently, Travaglio et al. (2001) adopted a mean of the Pb production by AGB models with different amounts of ^{13}C. Our results for two very metal-poor stars, in which the abundance ratios of neutron capture elements produced by AGB stars are well preserved, place strong constraints on the parameters for AGB stars with [Fe/H] ~ -2.7. In fact, the ratio [Pb/Ba] $= -0.19 \pm 0.28$ in LP 625-44 requires a smaller amount of ^{13}C than that of the so-called standard model with this metallicity (Ryan et al. 2001). The ratio is slightly higher in LP 706-7, [Pb/Ba] $= 0.27 \pm 0.24$. This may indicate that a range of ^{13}C amounts is indeed required in the most metal-poor AGB stars, as well as for the moderately metal-poor ones. However, the observational errors in the present study are sufficiently large that the difference between these two stars is only marginally significant. Hence, continued observational study of abundance ratios for neutron capture elements, in particular of Pb, in stars such as LP 625-44 and LP 706-7 (over a range of metallicity), is indispensable. These studies are necessary, both to refine models of stellar structure and evolution and to clarify the enrichment mechanism for neutron capture elements in the Galaxy.

We have pointed out that there is another possibility for the synthesis of *s*-process elements in the AGB stars, i.e., with nucleosynthesis taking place during thermal pulses, as discussed in the previous section. Further studies of this process are also important to understand better the enrichment of Pb in the Galaxy.

5. SUMMARY AND CONCLUDING REMARKS

From an analysis of high-resolution spectra, the Pb I $\lambda4057$ line is detected in the *s*-process–rich, very metal-poor subgiants LP 625-44 and LP 706-7. Since the overabundance of neutron capture elements in LP 625-44 (and possibly in LP 706-7) can be attributed to the mass transfer from companion AGB stars, their heavy-element abundance ratios provide a unique opportunity to investigate *s*-process nucleosynthesis in AGB stars at very low metallicity. The abundance ratios Ba/Sr and Pb/Ba are especially strong tools to constrain the parameters of classical *s*-

process models. In the context of these models, we have estimated the neutron exposure per pulse $\tau \sim 0.7$ mbarn^{-1}, a value significantly larger than that which best fits solar system material ($\tau \sim 0.4$), but consistent with the values predicted by models of rather metal-deficient AGB stars (Gallino et al. 1998). However, we also found that these abundance ratios can be explained by very high neutron density ($N_n \sim 10^{11}$ cm^{-1}), as well as low ones ($N_n \sim 10^7$ cm^{-1}). Further theoretical studies of evolved stars are required to distinguish nucleosynthesis pathways during thermal pulses from those that take place during the interpulse phase of AGB stars, as well as to identify which of these two is the more viable site for *s*-process nucleosynthesis at low metallicity.

To underpin these studies, accurate abundance analyses for similar *s*-process–rich, metal-poor, carbon-enhanced stars are required. In the present study, we have extended the abundance analysis, including the effects of hyperfine splitting and isotope shifts, to many lines of neutron capture elements, including Pb. These effects are important, not only in the determination of elemental abundances but also in the estimation of isotope ratios of some elements, when higher resolution and higher quality spectra become available. Further abundance studies of neutron capture–rich stars will reveal the characteristics of the *s*-process at low metallicity, such as its metallicity dependence, and the history of enrichment of neutron capture elements in the early Galaxy.

The authors wish to thank the Australian Time Assignment Committee and the Director and staff of the Anglo-Australian Telescope for the provision of research facilities. S. G. R. records his deep gratitude to R. Gallino, M. Busso, and C. Travaglio for numerous discussions on this topic and for their hospitality during a recent visit to Torino. S. G. R. was supported by PPARC grant PPA/O/S/1998/00658. W. A., H. A., and T. K. were supported in part by the Grant-in-Aid for Science Research 10044103, 10640236, and 12047233 of the Ministry of Education, Science, Sports, and Culture of Japan. G. J. M. was supported by DoE Nuclear Theory grant DE-FG02-95-ER40394 at the University of North Dakota. T. C. B. received partial support from NSF grant AST 00-98549. T. C. B. would also like to acknowledge support from a visiting scholar fellowship at the National Observatory of Japan and the hospitality of his hosts during his visit.

APPENDIX A

ISOTOPE SHIFTS AND HYPERFINE SPLITTING OF OBSERVED TRANSITIONS

Many of the elements beyond iron have multiple stable isotopes, giving rise in some cases to isotope shifts that are large enough to affect the formation of stellar spectral lines. Furthermore, if either the atomic number Z or the neutron number N of an isotope is odd, then hyperfine splitting is also possible. Isotope shifts and hyperfine splitting affect spectral line formation in the same way. Their effects are negligible for genuinely "weak" spectral lines, where the line strength varies linearly with the line opacity, but once a line begins to saturate and the relationship becomes nonlinear, as it is for many spectral lines, the wavelength distribution of the opacity becomes important. If a spectral line consists of multiple components whose separation is comparable to or greater than the intrinsic width of the line from natural, thermal, collisional, and microturbulent (but not macroturbulent) broadening, then line splitting can be important. Optical lines, even with equivalent widths as small as 20 mÅ, can be affected if the splitting is large enough.

Because line splitting affects the strength of a stellar spectral line, it also affects the abundances we compute. Neglect of line splitting in the computation of a spectral line results in an underestimate of the equivalent width and hence an overestimate of the abundance. If the relative intensities and separations of the components of the line are known, it is straightforward to calculate the impact of the splitting on the abundance. For the astronomer, the problem is a purely practical one: in many cases, the line separations of different isotopes and/or the splitting coefficients associated with hyperfine structure, for the transitions we wish to measure in stars, are simply unknown.

The hyperfine splitting of each energy level of a transition is characterized by the quantum number F, where F takes the values $I + J, I + J - 1, \ldots, |I - J|$, I being the nuclear spin quantum number and J being the electronic angular momentum quantum number, both of which are known. These quantum numbers determine the number of components into which a given level is split and also the relative intensities of the resulting lines. These values are relatively straightforward to obtain. The energy separations within each of the upper and lower levels are characterized by two hyperfine splitting coefficients A and B, but in many cases these are not known for transitions of interest. Where they are known, splittings can be computed as described, for example, by McWilliam et al. (1995).

In this appendix we report what is known about the lines of the rare earth elements and several others measured in our study. For many of the levels involved in the transitions we observed, only the A constant is known. This is not particularly troublesome, as the impact of the B constant on the level splitting is usually much smaller than that of A. In all cases in which the B value was not available, we assumed it to be zero. Below, we provide tables of wavelengths and the fraction of the total *gf*-value that should be assigned to each component. Some lines are included in this appendix that do not feature in Table 2. This is because not all lines were used in the final analysis, for reasons discussed in the main text. We nevertheless tabulate the components we calculated.

A1. LANTHANUM: PURE HYPERFINE SPLITTING

Lanthanum has only one stable isotope, ^{139}La, and although ^{138}La has a half-life of 1.12×10^{11} yr, in the solar system it accounts for less than 0.1% of the element. Consequently, the lighter isotope can be ignored. However, La has an odd Z and hence nonzero nuclear spin [$I(^{139}\mathrm{La}) = 7/2$], giving rise to hyperfine splitting (see Table A1).

TABLE A1

LANTHANUM HYPERFINE SPLITTING

This table is available only on-line as a machine-readable table.

Unfortunately, for most of the La transitions in our star, only the lower energy levels have published A values. In these cases we were forced to assume that the A value for the upper level was zero. This assumption, made necessary by the lack of data, means that our calculations of hyperfine splitting for La are imperfect. However, it is quite common (though not universal) for A values of the higher energy levels of optical lines to be lower by a factor of 5 or 10 than the lower energy level, so the assumption may not be too troublesome. More to the point, although we have had to make undesirable assumptions in order to make progress, the inclusion of lower level splittings means that our calculations are at least expected to be closer to reality than if we had neglected hyperfine splitting completely. A values were taken from Höhle, Hühnermann, & Wagner (1982). No values were available for the λ4619 transition. New measurements of hyperfine splitting for La, to address the lack of data, have been made and will be published separately (L. A. J. Blake & S. G. Ryan 2001, in preparation).

A2. CERIUM

Cerium has an even Z and all of the isotopes have even N, so the nuclear spin and hence hyperfine splitting are zero. Nevertheless, isotopic splitting is possible. There are four isotopes, though only two are significant in the solar system, with fractions ^{140}Ce = 88.5% and ^{142}Ce = 11.1%. Brix & Kopfermann (1952) list the isotope splittings for nine Ce II lines, six of which occur in our spectra. They have wavelengths from 4450 to 4628 Å and lower excitation energies, from 0.5 to 0.9 eV. In all cases, the ^{142}Ce lines lie 0.011 Å redward of ^{140}Ce. In the absence of information on the (many) remaining lines in our list, we applied this splitting to all of our Ce lines and apportioned the *gf*-value 89% to ^{140}Ce and 11% to ^{142}Ce. This shift approximation will not be exact but is likely to be better than assuming no splitting at all. As such a simple splitting scheme has been adopted, we refrain from publishing the Ce II line list.

A3. PRASEODYMIUM

Praseodymium has only a single isotope, so there is no isotope splitting, but the odd Z leads to a nonzero nuclear spin $I = 5/2$ and nonzero hyperfine splitting (see Table A2). Values of the splitting coefficient A were taken from Ginibre (1989). In some cases the splittings are comparable to the (large) splittings of Eu II.

A4. NEODYMIUM

Neodymium ($Z = 60$) has seven stable isotopes, two of which have odd N: ^{143}Nd makes up 12% in the solar system, and ^{145}Nd makes up 8%. The remaining isotopes have no hyperfine splitting, but isotopic shifts will affect all of them (see Table A3). Isotopic shifts between ^{144}Nd and ^{150}Nd were taken from Blaise et al. (1984). The shifts of other isotopes are derived from interval ratios, which for Nd are nonuniform. The spacing intervals from ^{144}Nd relative to the interval ^{144}Nd–^{150}Nd are Δ(142, 143, 144, 145, 146, 148, 150) = (−0.24, −0.15, 0.00, 0.06, 0.27, 0.56, 1.00) (Murakawa 1954). Solar system isotope ratios ^{142}Nd:^{143}Nd:^{144}Nd:^{145}Nd:^{146}Nd:^{148}Nd:^{150}Nd = 27:12:24:8:17:6:6 were used.

Our initial line lists were computed before Murakawa's work was identified, using the ratios (−0.29, −0.15, 0.00, 0.15, 0.33, 0.66, 1.00). As the differences are small, we did not reanalyze the stars using the revised splitting ratios. Nevertheless, the updated table is given below. Murakawa (1954) also provides hyperfine splitting constants for the ^{143}Nd and ^{145}Nd isotopes, but only for just over a quarter of the lines, and even then only for their lower levels. Within the limits of such patchy data, it appeared that the hyperfine splitting would still be considerably less than the isotope splitting, and without more complete information, the decision was taken to neglect the hyperfine splitting, especially since it would affect only 20% of the isotopic composition.

TABLE A2

PRASEODYMIUM HYPERFINE SPLITTING

This table is available only on-line as a machine-readable table.

TABLE A3

NEODYMIUM ISOTOPE SPLITTING

This table is available only on-line as a machine-readable table.

TABLE A4

SAMARIUM ISOTOPE SPLITTING

This table is available only on-line as a machine-readable table.

TABLE A5

EUROPIUM HYPERFINE AND ISOTOPE SPLITTING

This table is available only on-line as a machine-readable table.

A5. SAMARIUM

Samarium ($Z = 62$) has seven stable isotopes. Two of these, making up 29% of the solar system composition of the element, have odd N, but there are few data on the hyperfine splitting, so we confined our calculations to the isotope shifts (see Table A4). We assumed the solar system isotope ratios ^{144}Sm:^{147}Sm:^{148}Sm:^{149}Sm:^{150}Sm:^{152}Sm:^{154}Sm = 3:15:11:14:7:27:23. Shifts between the ^{148}Sm and ^{154}Sm isotopes were taken from Rao et al. (1990), and in four cases shifts between the ^{152}Sm and ^{154}Sm isotopes were from Brix & Kopfermann (1949, 1952). The splitting intervals, which are very nonuniform for Sm, were from Villemoes et al. (1995). For seven of our lines, no isotope shift data were found. The line lists for the remainder are tabulated below. For the lines at 3941 and 3979 Å, the isotope splitting is genuinely zero.

A6. EUROPIUM

Eu has only two isotopes, but as Z is odd ($Z = 63$), hyperfine splitting affects both of them. The magnetic moments of the two nuclei are $\mu_{151} = 3.46$ and $\mu_{153} = 1.53$, and the ratio between these gives the ratio of the hyperfine structure coefficients, $A_{151}/A_{153} = \mu_{151}/\mu_{153} = 2.26$ (e.g., Hauge 1972). That is, the hyperfine splitting of ^{151}Eu is approximately twice as large as the splitting of ^{153}Eu. A coefficients for our lines were taken from Krebs & Winkler (1960), if necessary using the ratio of magnetic moments to obtain coefficients for ^{153}Eu from the ^{151}Eu values. No coefficient could be found for the upper level of the λ3907 line; this was assumed to be zero (see earlier comments for La about this assumption). The line lists are given in Table A5.

The solar system isotope ratio is ^{151}Eu = 49%, ^{153}Eu = 51%, so we have adopted a simple 50:50 division of the gf-values. This resembles a pure r-process for which ^{151}Eu/^{153}Eu = 0.96, but, as discussed in the main text, the isotope mix for a pure s-process may be almost pure ^{153}Eu, whose line splitting is 2.26 times less than for ^{151}Eu. The line list provided can be modified for unequal isotope ratios simply by rescaling the gf-values. For example, a pure ^{153}Eu line list would be obtained by setting the ^{151}Eu "Frac." values in Table A5 to zero and doubling the ^{153}Eu values.

A7. LEAD

Lead ($Z = 82$) has four isotopes, one of which (^{207}Pb) has an odd neutron number (see Table A6). Isotope shift data were taken from Manning, Anderson, & Watson (1950) and gf-values apportioned according to the solar system isotope ratios (^{204}Pb:^{206}Pb:^{207}Pb:^{208}Pb = 0.015:0.236:0.226:0.523). Manning et al. (1950) list the isotope splittings and intensities for three components of ^{207}Pb due to the hyperfine splitting of the λ4057 line but provide only the center of gravity for the ^{207}Pb component of the λ3739 line; this accounts for the different numbers of components we list below.

TABLE A6

LEAD HYPERFINE AND ISOTOPE SPLITTING

This table is available only on-line as a machine-readable table.

REFERENCES

Allen, C., & Santillan, A. 1991, Rev. Mexicana Astron. Astrofis., 22, 255

Aoki, W., Norris, J. E., Ryan, S. G., Beers, T. C., & Ando, H. 2000, ApJ, 536, L97 (Paper I)

Aoki, W., & Tsuji, T. 1997, A&A, 328, 175

Arlandini, C., Käppeler, F., Wisshak, K., Gallino, R., Lugaro, M., Busso, M., & Straniero, O. 1999, ApJ, 525, 886

Bao, Z. Y., Beer, H., Käppeler, F., Voss, F., Wisshak, K., & Rauscher, T. 2000, At. Data Nucl. Data Tables, 76, 70

Baushlicher, C. W., Jr., Langhoff, S. R., & Taylor, P. R. 1988, ApJ, 332, 531

Bergström, H., Biémont, E., Lundberg, H., & Persson, A. 1988, A&A, 192, 335

Biémont, E., Garnir, H. P., Palmeri, P., Li, Z. S., & Svanberg, S. 2000, MNRAS, 312, 116

Biémont, E., Grevesse, N., Hannaford, P., & Lowe, R. M. 1981, ApJ, 248, 867

———. 1989, A&A, 222, 307

Biémont, E., Karner, C., Meyer, G., Träger, F., & zu Putlitz, G. 1982, A&A, 107, 166

Blaise, J., Wyart, J.-F., Djerad, M. T., & Ahmed, Z. B. 1984, Phys. Scr., 29, 119

Bord, D. J., Barisciano, L. P., & Cowley, C. R. 1996, MNRAS, 278, 997

Brix, P., & Kopfermann, H. 1949, Z. Phys. D, 126, 344

———. 1952, Landolt-Bornstein I, 5, 39

Busso, M., Gallino, R., & Wasserburg, G. J. 1999, ARA&A, 37, 239

Cameron, A. G. W. 1955, ApJ, 121, 144

———. 1960, ApJ, 131, 521

Corliss, C. H., & Bozman, W. R. 1962, Experimental Transition Probabilities for Spectral Lines of Seventy Elements (NBS Monograph 53; Washington: GPO)

ESA 1997, The *Hipparcos* and Tycho Catalogues, ESA SP-1200

Fujimoto, M. Y., Ikeda, Y., & Iben, I., Jr. 2000, ApJ, 529, L25

Gallino, R., Arlandini, C., Busso, M., Lugaro, M., Travaglio, C., Straniero, O., Chieffi, A., & Limongi, M. 1998, ApJ, 497, 388

Gilroy, K., Sneden, C., Pilachowski, C. A., & Cowan, J. J. 1988, ApJ, 327, 298

Ginibre, A. 1989, Phys. Scr., 39, 694

Goly, A., Kusz, J., Nguyen Quang, B., & Weniger, S. 1991, J. Quant. Spectrosc. Radiat. Transfer, 45, 157

Goriely, S., & Mowlavi, N. 2000, A&A, 362, 599

Gratton, R. G., & Sneden, C. 1994, A&A, 287, 927

Hauge, O. 1972, Inst. Theor. Ap. Oslo, Rep. 35

Herwig, F., Bloecker, T., Schoenberner, D., & El Eid, M. 1997, A&A, 324, L81

Höhle, C., Hühnermann, H., & Wagner, H. 1982, Z. Phys. A, 304, 279

Howard, W. M., Mathews, G. J., Takahashi, K., & Ward, R. A. 1986, ApJ, 309, 633

Iben, I. 1977, ApJ, 217, 788

Irwin, A. W. 1981, ApJS, 45, 621

Käppeler, F., Beer, H., & Wisshak, K. 1989, Rep. Prog. Phys., 52, 945

Krebs, K., & Winkler, R. 1960, Z. Phys., 160, 320

Kurucz, R. L. 1993, CD-ROM 13, ATLAS 9 Stellar Atmospheres Programs and 2 km/s Grid (Cambridge: SAO)

Kusz, J. 1992, A&AS, 92, 517

Langer, N., Heger, A., Wellstein, S., & Herwig, F. 1999, A&A, 346, L37

Maier, R. S., & Whaling, W. 1977, J. Quant. Spectrosc. Radiat. Transfer, 18, 501

Manning, T. E., Anderson, C. E., & Watson, W. W. 1950, Phys. Rev., 78, 417

Mathews, G. J., Bazan, G., & Cowan, J. J. 1992, ApJ, 391, 719
Mathews, G. J., & Ward, R. A. 1985, Rep. Prog. Phys., 48, 1371
McWilliam, A. 1998, AJ, 115, 1640
McWilliam, A., Preston, G. W., Sneden, C., & Searle, L. 1995, AJ, 109, 2757
Murakawa, K. 1954, Phys. Rev., 96, 1543
Norris, J. E., Ryan, S. G., & Beers, T. C. 1996, ApJS, 107, 391
———. 1997a, ApJ, 488, 350
———. 1997b, ApJ, 489, L169
Preston, G. W., & Sneden, C. 2001, AJ, in press
Rao, P. M., Ahmad, S. A., Venugopalan, A., & Saksena, G. D. 1990, Z. Phys. D, 15, 211
Rayet, M., & Hashimoto, M. 2000, A&A, 354, 740
Reeves, H. 1966, ApJ, 146, 447
Ryan, S. G., Aoki, W., Norris, J. E., Beers, T. C., Gallino, R., Busso, M., & Ando, H. 2001, Nucl. Phys. A, 688, 209
Ryan, S. G., & Norris, J. E. 1991, AJ, 101, 1835
Ryan, S. G., Norris, J. E., & Beers, T. C. 1996, ApJ, 471, 254
Sclattl, H., Cassisi, S., Salaris, M., & Weiss, A. 2001, ApJ, submitted
Sneden, C., McWilliam, A., Preston, G. W., Cowan, J. J., Burris, D. L., & Armosky, B. J. 1996, ApJ, 467, 819
Spite, M., & Spite, F. 1978, A&A, 67, 23
Straniero, O., Gallino, R., Busso, M., Chieffi, A., Raiteri, C. M., Limongi, M., & Salaris, M. 1995, ApJ, 440, L85
The, L.-S., El Eid, M. F., & Meyer, B. S. 2000, ApJ, 533, 998
Travaglio, C., Gallino, R., Busso, M., & Gratton, R. 2001, ApJ, 549, 346
Truran, J. W. 1981, A&A, 97, 391
Villemoes, P., Wang, M., Arnesen, A., Weiler, C., & Wännström, A. 1995, Phys. Rev. A, 51, 2838
Ward, L., Vogel, O., Arnesen, A., Hallin, R., & Wännström, A. 1985, Phys. Scr., 31, 161
Youssef, N. H., & Khalil, N. M. 1989, A&A, 208, 271
Zachwieja, M. 1995, J. Mol. Spectrosc., 170, 285
———. 1997, J. Mol. Spectrosc., 182, 18